The Thesis Committee for Mauro Ariel Palavecino
Certifies that this is the approved version of the following thesis:

New Methods of Petrophysical Rock Classification Based on MICP and Grain-Size Distribution Measurements with Applications in Carbonates and Tight-Gas Sandstones

APPROVED BY
SUPERVISING COMMITTEE:

Supervisor:

Carlos Torres-Verdín

Zoya Heidari

New Methods of Petrophysical Rock Classification Based on MICP and Grain-Size Distribution Measurements with Applications in Carbonates and Tight-Gas Sandstones

by

Mauro Ariel Palavecino, B.Eng.

Thesis

Presented to the Faculty of the Graduate School of

The University of Texas at Austin

in Partial Fulfillment

of the Requirements

for the Degree of

Master of Science in Engineering

The University of Texas at Austin

December 2016

Acknowledgements

First and foremost, I would like to thank Dr. Carlos Torres-Verdín for his continued guidance and support throughout my research work. He introduced me to the amazing field of petrophysics and shared his invaluable knowledge with patience and dedication. I am thankful that Carlos believed in my capability to succeed in this challenging and prestigious graduate program and I will be forever in debt to him for this opportunity.

Secondly, I would like to thank Dr. Zoya Heidari for agreeing to be the reader of this thesis and for providing thorough comments and feedback to my work.

I would like to thank all of the sponsors of the Formation Evaluation Research Consortium for funding this research work and my graduate education: AkerBP, Anadarko, Aramco, Baker-Hughes, BHP Billiton, BP, China Oilfield Services LTD., ConocoPhillips, DEA, ENI, ExxonMobil, Hess, Inpex, Paradigm, Petrobras, Repsol, Schlumberger, Shell, Southwestern, Statoil, TOTAL, Wintershall and Woodside Petroleum Limited.

Additionally, I want to thank the Osmar Abib Endowed Presidential Scholarship and the Abib family for their generous support during my two years of studies.

I am very grateful to the Formation Evaluation Research Consortium staff including Rey Casanova, Dr. Roger Terzian, Dr. Joaquin Ambia-Garrido, Dr. David Medellin, Dr. Wilberth Herrera, and Dr. Bruce Klappauf. Their support and assistance throughout these two years has been invaluable.

I would also like to thank all my co-workers and fellow students. A special thanks goes to Juan Diego and Colin, whose friendship made the office time more enjoyable.

I cannot forget about my friends in Austin: Mayra, Franco, Marito, Chino, and Delfi, for being our family while abroad and for sharing unforgettable moments together.

I want to thank all my family for the unwavering support and encouragement that they provided throughout the entire experience. I am very lucky to have such great in-laws, Dani and Lili, who were always interested and supportive of my studies and research. Thanks also to Pili, for her unconditional support. To the best sister of all, Cris, and of course to my parents, Pa y Ma, whose hard work made it possible for me to be here today.

Finally, I want to thank my beautiful wife, Lu, for sharing this adventure with me. None of this would have been possible without you being by my side.

Abstract

New Methods of Petrophysical Rock Classification Based on MICP and Grain-Size Distribution Measurements with Applications in Carbonates and Tight-Gas Sandstones

Mauro Ariel Palavecino, M.S.E.

The University of Texas at Austin, 2016

Supervisor: Carlos Torres-Verdín

Rocks that exhibit bimodal throat-size distributions cannot be reliably appraised and classified using classical techniques such as the Winland R35 method (Pittman, 1992) or Amaefule's flow zone indicator (Amaefule et al., 1993). These popular classification procedures/protocols are based on the assumption that rocks exhibit a single dominant throat size, and they fail to account for the bimodal nature of pore throat-size distributions. Carbonates and tight-gas sandstones are notorious for exhibiting non-unimodal throat-size distributions and extreme spatial variability. In addition, wide variations of throat sizes are often observed in rocks that have been subject to extreme diagenesis and recrystallization.

This thesis introduces new methods for classifying and grouping rocks based on mercury-intrusion capillary pressure (MICP) and grain-size distribution measurements. I use various canonical basis functions to reproduce logarithmic throat-size and grain-size distributions derived from MICP data and grain-size distribution measurements. A bimodal

logarithmic Lorentzian distribution is introduced to model the rock's throat and grain-size distributions. The functions' free parameters are used to establish correlations with permeability and irreducible water saturation. In cases where grain size data are available, I show how to estimate irreducible water saturation based on the effective surface-to-volume ratio of the rock. Results are then compared with bimodal logarithmic Gaussian distributions (Xu et al., 2013) and logarithmic Thomeer hyperbolas (Thomeer, 1960) to assess when each canonical description may or may not be more accurate than conventional methods for modeling the distribution of throat sizes and the corresponding flow properties. Finally, I introduce two new rock classification methods, which account for the rock's pore and throat-geometry parameters, that can be used to quantify storage and flow properties.

The new petrophysical description and classification methods are verified with several field examples. In the case of Bossier tight-gas sandstones, the methods are capable of identifying outlier permeability measurements and reliably classifying their storage and flow properties. Further, I demonstrate the importance of identifying the bimodal nature of the throat sizes with an example from the Panoma carbonate field. In this example a more accurate rock classification is obtained using the proposed method compared to the flow-zone indicator method. I also introduce an example from a siliciclastic sedimentary sequence located offshore Trinidad, where additional petrophysical data confirms that the bimodal nature of the grain-size distribution yields reliable estimates of irreducible water saturation. Finally, a second rock classification method that integrates grain topology, capillary pressure, and permeability is introduced and tested with data acquired in a tight-gas sandstone formation. The new petrophysical rock classification methods yield improved descriptions of throat and grain-size distributions, which result in more accurate calculations of permeability for rocks exhibiting complex pore-throat geometries.

Table of Contents

List of Figures

Chapter 1: Introduction

Rock classification and grouping is an important step in every reservoir modeling workflow. Proper identification of the different rock types present in a formation enables an improved estimation of dynamic petrophysical properties such as permeability. This results in a better assessment of rock productivity and a more accurate estimation of reserves. Many core-based rock typing methods exist and are widely used to achieve a better assessment of permeability than standard linear porosity-permeability correlations. Winland's R35 (Pittman, 1992) and Amaefule's flow zone indicator (Amaefule et al., 1993) are methods that have been demonstrated to yield good results when applied to conventional reservoirs where rocks exhibit a dominant throat/grain size. However, when rocks exhibit bimodal throat-size distributions, the aforementioned methods are unreliable since they tacitly imply a single, dominant throat/grain size. The necessity to introduce new methods that properly model bimodal throat sizes and enable a more reliable rock classification method for such complex rocks was the motivation for this thesis.

The central objective is the introduction of new methods for petrophysical rock classification based on core measurements. Specifically, the methods are based on data obtained from mercury-intrusion capillary pressure (MICP) and grain-size distribution measurements. New parametric models are introduced, which extend the concept of bimodal logarithmic Gaussian density functions of throat sizes (Xu et al., 2013). Throughout this work, three bimodal basis functions are examined to describe the variability of throat sizes. After modeling the MICP data or the grain-size distribution measurements with different functions, the main interest is to relate fitted parameters with relevant petrophysical properties. The bundle of capillary tubes model (Peters, 2012) is

used to correlate permeability and irreducible water saturation for the case of MICP modeling. Then, Timur's equation (Timur, 1968) is used in conjunction with the Kozeny-Carman model (Peters, 2012) to estimate irreducible water saturation and permeability from grain-size distribution measurements. Finally, I make use of the petrophysical descriptions associated with the three throat-size distribution parametric models to perform rock classification via K-means clustering (Press et al., 2007).

Two different rock typing approaches are introduced and verified using field samples. In the first method, modeled parameters for the basis functions are averaged to obtain characteristic means that are representative of the complete pore space. In the second method, each mode of the throat-size distribution is clustered independently to assess different rock types based on storage and flow properties.

Chapter 2: MICP and Grain-Size Distribution Modeling[1]

Simple canonical basis functions are invoked to model MICP data and grain-size distribution measurements. The basis functions are derived from classical probability models and other previously published models that were found to suitably reproduce complex pore and throat-space geometries. Three different basis functions are introduced: a bimodal Lorentzian distribution (Palavecino et al., 2016), a single or bimodal Thomeer hyperbola (Thomeer, 1960), and a bimodal Gaussian distribution (Xu et al., 2013).

2.1 Lorentzian Probability Density Function

The Lorentzian model is based on the Lorentzian probability density function (Johnson et al., 1994). I reproduce the MICP curve using a bimodal Lorentzian function. The calculation starts by converting capillary pressure to throat radius using the Washburn equation:

$$R = \frac{2\sigma\cos\theta}{P_c}, \tag{2.1}$$

where P_c is capillary pressure, σ is surface tension, and θ is contact angle. Next, the cumulative logarithmic Lorentzian distribution function is written as

$$S_w(\ln R; w_1, \gamma_1, R_{o1}; w_2, \gamma_2, R_{o2}) = w_1\left[\frac{1}{\pi}\tan^{-1}\left(\frac{\ln R - \ln R_{o1}}{\gamma_1}\right)+\frac{1}{2}\right]+$$
$$+w_2\left[\frac{1}{\pi}\tan^{-1}\left(\frac{\ln R - \ln R_{o2}}{\gamma_2}\right)+\frac{1}{2}\right], \tag{2.2}$$

where R is throat radius, R_{o1} and R_{o2} represent the mean throat radius of the large and small pore-space fractions, respectively, γ_1 and γ_2 are scale parameters, and w_1 and w_2 are pore-volume fractions. Equation (2.2) can be differentiated with respect to throat radius

[1] Content from this Chapter was previously published by the main author (Palavecino et al., 2016).

to obtain a density function which represents the throat-size distribution of the rock (Peters, 2012).

2.2 THOMEER AND GAUSSIAN MODELS

Using a similar approach, I reproduce the MICP data by fitting Thomeer hyperbolas (Thomeer, 1960). In the case of bimodal throat-size distributions, two Thomeer hyperbolas are implemented by adding the bulk volume fractions of the pore space via

$$BV(P_c; BV_{\infty 1}, G_1, P_{d1}; BV_{\infty 2}, G_2, P_{d2}) = BV_{\infty 1} e^{\left(-\frac{G_1}{\ln P_c - \ln P_{d1}}\right)} + BV_{\infty 2} e^{\left(-\frac{G_2}{\ln P_c - \ln P_{d2}}\right)}, \quad (2.3)$$

where P_c is capillary pressure, $BV_{\infty 1}$ and $BV_{\infty 2}$ represent the fraction of the pore space modeled by each hyperbola, G_1 and G_2 are pore-geometry factors, and P_{d1} and P_{d2} are displacement pressures corresponding to each hyperbola. Equation (2.3) can be differentiated with respect to throat radius to obtain the throat-size distribution.

The bimodal logarithmic Gaussian model (Xu et al., 2013) provides an additional method of reproducing both MICP and grain-size distribution data. The corresponding cumulative density function is given by

$$S_w(\ln R; w_1, \mu_1, \sigma_1; w_2, \mu_2, \sigma_2) = \frac{w_1}{2}\left[1 + erf\left(\frac{\ln R - \ln \mu_1}{2(\ln \sigma_1)^2}\right)\right] +$$

$$+ \frac{w_2}{2}\left[1 + erf\left(\frac{\ln R - \ln \mu_2}{2(\ln \sigma_2)^2}\right)\right], \quad (2.4)$$

where R is throat radius, μ_1 and μ_2 represent the mean throat radius of the large and small pore-space fractions, respectively, σ_1 and σ_2 are each mode's standard deviation parameters, and w_1 and w_2 are pore-volume fractions. Equation (2.4) can be also differentiated with respect to throat radius to obtain the throat-size distribution of the rock.

2.3 MICP Bimodal Throat-Size Distribution Modeling

Figure 2.1 shows an example of how MICP data is modeled for the case of rocks exhibiting bimodal throat-size distributions, such as those in the carbonate Panoma field of Kansas. The same figure shows the calculated throat-size distributions calculated using the three models described in this section.

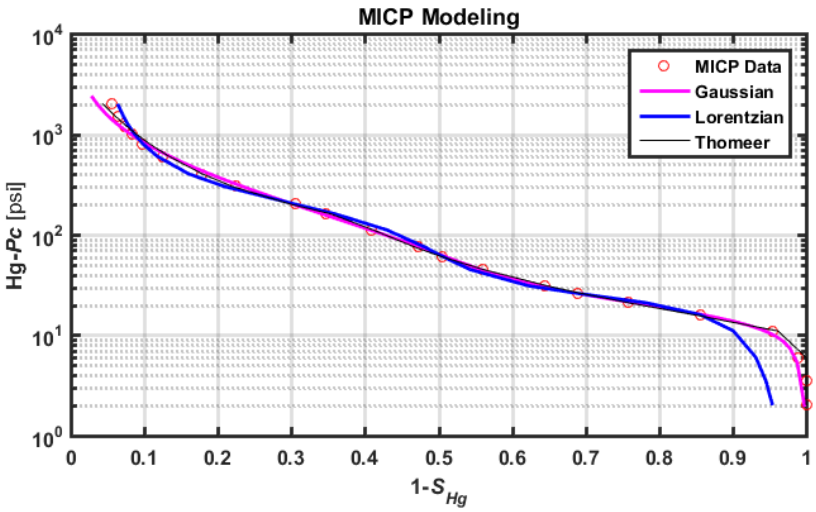

(a)

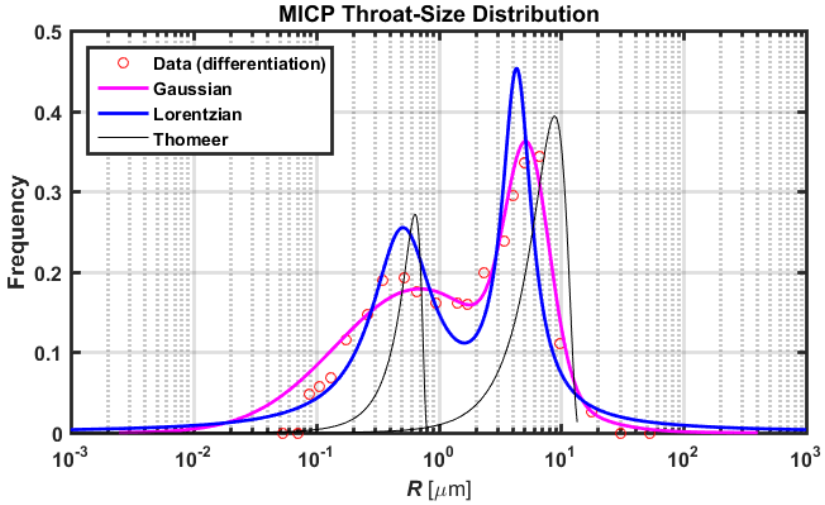

(b)

Figure 2.1: MICP modeling using three types of canonical basis functions. The cumulative distribution of the three logarithmic models: Gaussian, Lorentzian, and Thomeer are shown together with the experimental data in (a), where the x-axis shows one minus mercury saturation, and the y-axis shows the mercury capillary pressure. In (b), the three throat-size distribution models, which were calculated by taking the derivative of the corresponding capillary pressure models, are compared with the throat-size distribution of the rock.

2.4 Grain-Size Distribution Modeling

Figure 2.2 demonstrates how logarithmic grain-size distribution data is modeled using a Lorentzian and a Gaussian basis function. The data used for this example is from a unimodal sample acquired in a siliciclastic sedimentary sequence located offshore Trinidad. From the models three characteristic parameters are obtained: the distribution's mean, amplitude, and pore-volume fraction that is associated with each mean pore throat size. The petrophysical meaning of these parameters is examined in the following chapters.

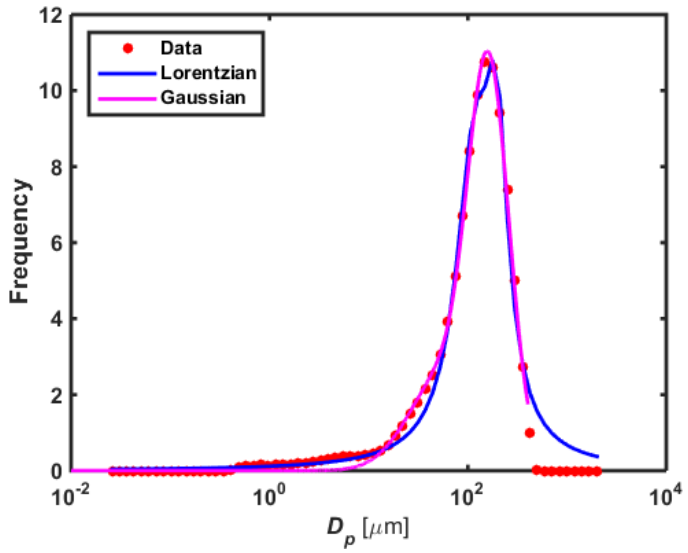

Figure 2.2: Grain-size distribution modeling of a unimodal sample from a siliciclastic sedimentary sequence located offshore Trinidad. Particle diameter is shown on the x-axis and the frequency is shown on the y-axis.

Chapter 3: Assessment of Permeability and Irreducible Water Saturation[2]

In this chapter, I examine the petrophysical meaning of the modeled parameters obtained in chapter 2 and associate them with salient petrophysical properties. The bundle of capillary tubes model is invoked to correlate the throat radius and amplitude of the distribution with the rock's permeability. Additionally, Timur-Tixier's equation is used to understand how the distribution's amplitude will affect the irreducible water saturation of the rock. In cases where grain size data is available, Kozeny-Carman's model is applied to estimate the permeability and irreducible water saturation of the rock.

3.1 Estimation of Permeability from MICP Modeling Parameters

After modeling MICP or grain-size distribution data, the interest shifts to associating the modeling parameters with petrophysical properties. In this first section the correlation between modeled parameters and the core-measured permeability is examined.

3.1.1 Bundle of Capillary Tubes Model

The bundle of capillary tubes model is applied to correlate permeability with the parameters estimated while fitting the MICP data. To improve the correlation a transformation of the bundle of capillary tubes model is invoked, which is given by

$$\ln k = \ln A_{bt} + B_{bt} \ln\left(\frac{\phi R_m^2}{\sqrt{\tau}}\right), \tag{3.1}$$

[2] Content from this Chapter was previously published by the main author (Palavecino et al., 2016).

where k is permeability, ϕ is porosity, τ is tortuosity, and R_m is mean throat radius. Using this equation a relationship between the modeling parameters and the rock's petrophysical properties is established. The mean throat radius in the bundle of capillary tubes model is replaced by the mean obtained by fitting the parametric model. Similarly, the tortuosity in equation (3.1) is replaced by the amplitude parameter from the parametric model.

When working with a rock that exhibits a bimodal throat-size distribution, I calculate characteristic parameters such as the mean throat radius and the amplitude of the distribution from the described models. This is performed using a weighted average and the pore-fraction parameter. For instance, to calculate the mean throat radius of a bimodal distribution, I use

$$R_m^2 = w_1 R_{o1}^2 + w_2 R_{o2}^2, \tag{3.2}$$

where R_m is the characteristic mean throat radius, w_1 and w_2 are the pore volume fractions of the large and small throats mode, respectively, and R_{o1} and R_{o2} are the large and small mean throat sizes, respectively.

Equation (3.2), which combines the fitting parameters associated with each of the mean throat sizes, is used to calculate a characteristic mean throat radius representing the complete rock sample. After testing different ways to average these values, an arithmetic average was found to yield the best correlation with empirical data.

3.1.2 Field Case 1: Panoma Carbonates

The Hugoton, Panoma, and Guymon fields, which together constitute the largest gas field in North America, contain an estimated ultimate recovery of 75 tcf of gas. Situated on the Hugoton embayment of the Anadarko basin, production from these fields originates from the lower Permian Chase and Council Grove Groups, which comprise a wide range

of lithofacies, including continental and marine siltstones, sandstones, mudstones, grainstone limestones, fine to medium-crystalline dolomites, and phylloid algal bafflestones (Dubois et al., 2006). For this study, publicly available laboratory measurements of 30 rock samples from the Panoma field were used to verify our models in carbonate rocks. Figure 3.1 shows an example of the correlation between measured (Klinkenberg-corrected) and estimated permeabilities for each of the three parametric models for rock samples acquired in the Panoma field.

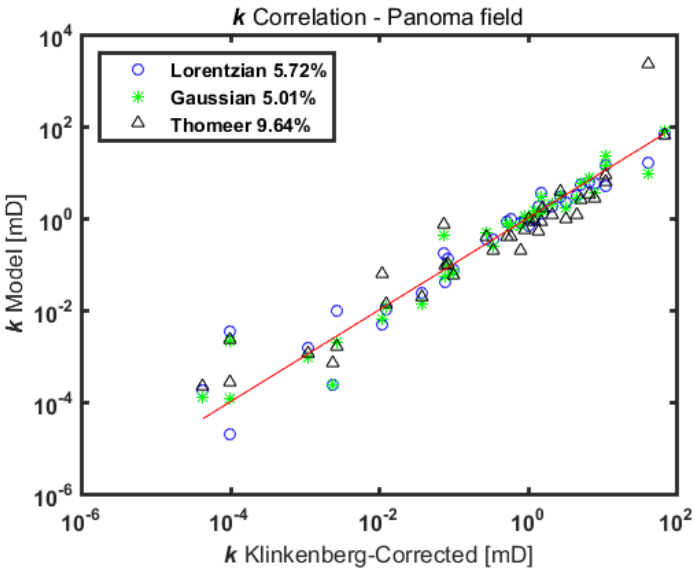

Figure 3.1: Correlation obtained between the model-estimated permeability the and Klinkenberg-corrected permeability.

3.2 ESTIMATION OF IRREDUCIBLE WATER SATURATION

3.2.1 Timur-Tixier Equation

I also examine the relationship between irreducible water saturation and estimated model parameters. Using Timur's equation (Timur, 1968) and the bundle of capillary tubes model, the following relationship is proposed to estimate irreducible water saturation ($S_{w,irr}$):

$$S_{w,irr} = C_{bt} \frac{\sqrt{\tau}}{R_m^2}. \tag{3.3}$$

The tortuosity value, τ, is replaced by the amplitude parameter from any of the MICP models, while the mean throat-radius, R_m, is replaced by the mean of the distribution. Figure 3.2 verifies equation (3.3) by comparing the estimated irreducible water saturation values from equation (3.3) with those estimated from NMR measurements.

3.2.2 Field Case 2: Bossier Tight-Gas Sandstone

The Bossier sandstone member of the Cotton-Valley group in East Texas is a thick, lithologically complex system containing interbedded shales with fine to very fine-grained argillaceous sandstones (Montgomery, 2000). Using equation (3.3), the correlation between model parameters and irreducible water saturation was examined. Figure 3.2 shows a good correlation between NMR-derived and calculated irreducible water saturation, which corroborates the fact that the fitting model parameters are intimately related to salient petrophysical properties.

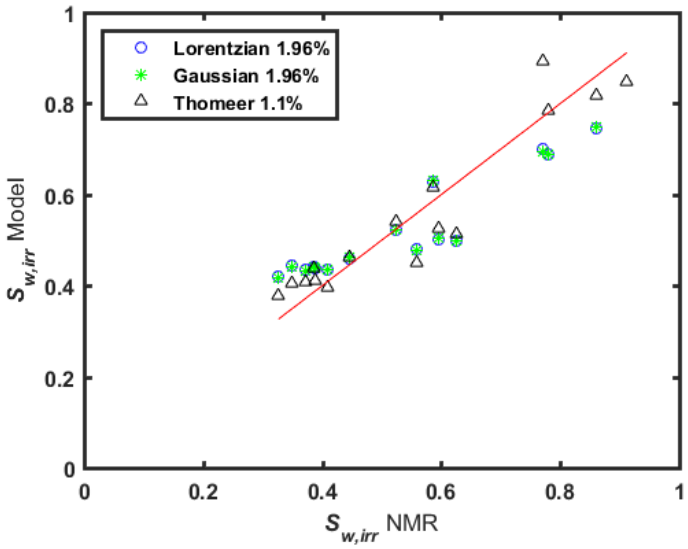

Figure 3.2: Comparison between the estimated irreducible water saturation values from equation (3.3) and those estimated from NMR measurements in a Bossier sandstone field case.

3.3 Permeability and Irreducible Water Saturation Estimation from Grain Size Data

A similar approach can be implemented to model grain-size distribution data. Lorentzian and Gaussian basis functions are used to reproduce the logarithmic grain-size distribution data. In this case, a mean grain diameter is calculated, which is the mean of the fitted distribution. In doing so, I also obtain an amplitude parameter, which is the standard deviation or the scale parameter, depending on the model used. The subsections below describe how the estimated parameters relate to relevant petrophysical properties.

3.3.1 Kozeny-Carman Permeability Model

I use the Kozeny-Carman equation to derive a permeability relationship that considers the mean grain diameter and the tortuosity, which is replaced with the model's amplitude parameter. The derived relationships is given by

$$\ln k = \ln A_{kc} + B_{kc} \ln\left(\frac{D_{pm}{}^2 \phi^3}{\tau(1-\phi)^2}\right), \tag{3.4}$$

where D_{pm} is average grain diameter, ϕ is porosity of the rock, τ is tortuosity, and k is permeability of the rock.

3.3.2 Irreducible Water Saturation Estimation

Timur's equation relates permeability with porosity and irreducible water saturation. It was shown above that the mean grain diameter and the amplitude parameters can be used to accurately estimate permeability from grain size data. I obtain an expression to estimate irreducible water saturation after equating Timur's equation to Kozeny-Carman's permeability model, given by

$$S_{w,irr} = C_{kc} \frac{(1-\phi)}{D_{pm}} \sqrt{\tau \phi^{1.4}} \ . \tag{3.5}$$

In equation (3.5) the mean grain-diameter is replaced by the mean of the selected model and the tortuosity is replaced by the model's amplitude parameter. Equation (3.5) can be used for the estimation of irreducible water saturation.

3.3.3 Field Case 3: Offshore Trinidad

Figure 3.3 shows how equation (3.4) accurately reproduces the permeability when using the parameters obtained from the grain-size distribution fit. The data shown originated from a siliciclastic sedimentary sequence located offshore Trinidad.

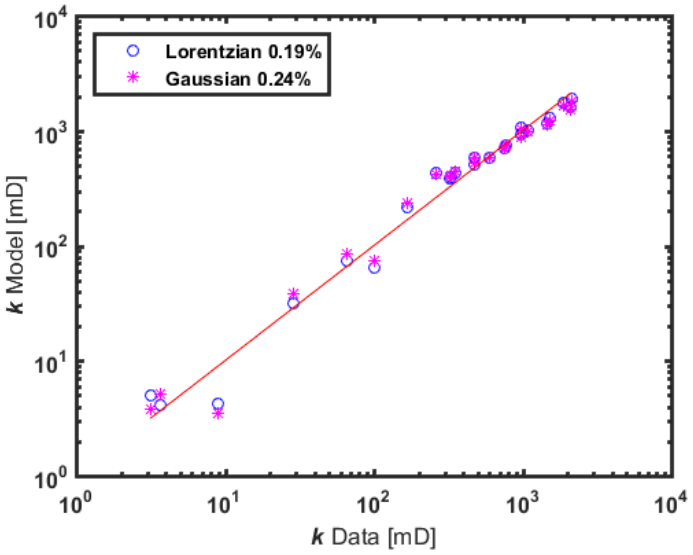

Figure 3.3: Permeability estimation from grain-size distribution data in a siliciclastic sedimentary sequence located offshore Trinidad.

It is worth emphasizing the importance of the introduced parametric models when implemented on rock samples that exhibit bimodal grain-size distributions. Figure 3.4 displays estimates of irreducible water saturation for the Trinidad field case that were calculated using equation (3.5). An outlier point can be observed with abnormally high irreducible water saturation compared to the rest of the data. Based on the associated grain-size distribution data shown in Fig. 3.5, where the outlier's distribution is highlighted in red, it was observed that this sample exhibited a bimodal grain-size distribution. The presence of the second, smaller grain size mode, which was not observed in any of the other samples, likely led to the relatively high irreducible water saturation.

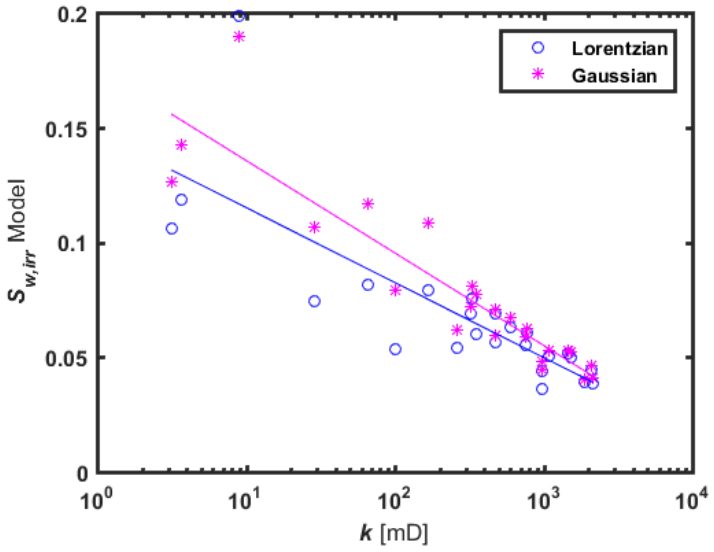

Figure 3.4: Irreducible water saturation estimation using Kozeny-Carman's approach. An outlier point with higher irreducible water saturation stands out from the rest of the dataset.

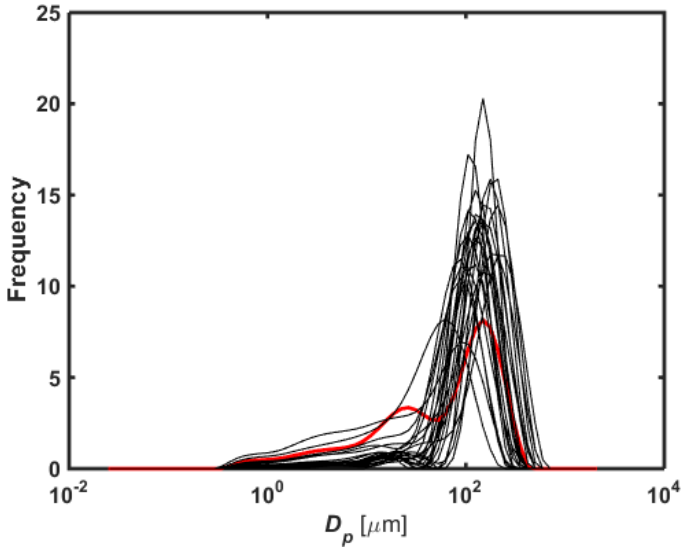

Figure 3.5: Grain-size distribution data for all the samples obtained from the offshore Trinidad field. The highlighted curve in red corresponds with the outlier point observed in Fig. 3.4. This sample has a higher fraction of small grains, which is why the irreducible water saturation is higher than the rest of the data.

Chapter 4: Grain Topology Analysis in Rocks with Multiple Grain Sizes

Bimodal throat-size distributions can be attributed to different pore-space geometric descriptions, depending on the lithology and geological setting of a rock. In carbonate rocks, a bimodal throat-size distribution is associated with differential dissolution of the matrix, which results in two different pore systems that are usually named macropores and micropores. In a fractured system, a bimodal throat-size distribution can be associated with the fractures and the matrix. Finally, in a siliciclastic sedimentary rock, a bimodal throat-size distribution is associated with the presence of different grain sizes.

In this chapter, I present the relationship between grain topology and capillary pressure in clastic rocks with variable grain sizes. I also present equations for calculating the effective permeability of these variable grain size systems. The importance of understanding the grain topology of clastic rocks with variable grain sizes is included in the second rock classification method, which is introduced in the following chapter.

4.1 Calculation of Permeability in Rocks With Variable Grain Sizes

In clastic rocks, it is widely understood that shale concentration affects permeability. In a shale-sandstone laminated system, effective permeability can be calculated using a weighted average of the sandstone and shale concentrations. For dispersed shale-sandstone systems, the following equation can be invoked to calculate effective permeability (Revil et al., 1999):

$$k_{sd-sh} = k_{sd}\left[1 - C_{sh}\left(\frac{1-\phi_{sh}}{\phi_{sd}}\right)\right]^{3m_{cs}}, \tag{4.1}$$

where k_{sd-sh} is effective permeability of the shaly-sandstone system, k_{sd} is permeability of the sandstone, ϕ_{sd} is porosity of the sandstone, ϕ_{sh} is porosity of the shale, C_{sh} is shale concentration, and m_{cs} is cementation exponent of a specific rock.

In cases where more than one rock type (or grain size) is present in a given sample, the way that these different grain sizes are arranged in space affects the calculation of effective permeability. In this section, I present the equations used to calculate effective permeability in shale-sandstone systems, where shale and two different sandstone types are present in the same formation.

4.1.1 Laminated grain types and shale systems

When two different rock types are present in a laminated system, the effective permeability is simply a weighted average of the individual permeability of each rock type, which can be described by

$$k_h = (1-C_{sh})[w_1 k_{s1} + w_2 k_{s2}] + C_{sh} k_{sh} \quad , \tag{4.2}$$

where k_h is effective permeability parallel to the bedding plane, k_{s1} and k_{s2} are the permeability of each sandstone type, w_1 and w_2 are sandstone type volumetric fractions, k_{sh} is shale permeability, and C_{sh} is shale concentration. Alternatively, an equation for the permeability perpendicular to the bedding plane can be obtained using

$$\frac{1}{k_v} = (1-C_{sh}) \frac{w_1 k_{s2} + w_2 k_{s1}}{k_{s1} k_{s2}} + \frac{C_{sh}}{k_{sh}} \quad , \tag{4.3}$$

where k_v is effective permeability perpendicular to bedding plane.

4.1.2 Dispersed grain types and shale systems

For dispersed systems, I invoke Revil's model for shaly-sands (Revil et al., 1999) and expand it to consider mixed-sandstone-shale systems. Equation (4.1) describes the effective permeability for a system with shale and a single sandstone type. If the permeability of the sandstone is replaced by the permeability of the sandstone with mixed grains, then the following equation is obtained:

$$k_{sd12-sh} = k_{sd12}\left[1 - C_{sh}\left(\frac{1-\phi_{sh}}{\phi_{sd12}}\right)\right]^{3m_{cs12}} , \tag{4.4}$$

where $k_{sd12-sh}$ is effective permeability of the mixed-sandstone-shale system, k_{sd12} is effective permeability of the sandstone fraction, ϕ_{sd12} is porosity of the mixed-sandstone system, and ϕ_{sh} is shale porosity. The parameter m_{cs12} is the cementation exponent of the mixed-sandstone-shale system.

Given the permeability and porosity of each rock type, the only unknown in equation (4.4) is the cementation exponent, which is specific to each sandstone-shale type. Because the scope of this study is to understand the behavior of permeability in mixed systems, synthetic rock types were constructed containing different proportions of sandstone grain sizes and shale concentrations using the Pore Level Petrophysics module of The University of Texas at Austin Petrophysical and Well-Log Simulator (Shabro, 2013, and Torskaya, 2014). To accomplish this, two simplified grain-packs were constructed and then combined in different proportions. Subsequently, a cement concentration was added to the digital rocks in a grain-coating fashion, which serves an approximation for dispersed shale concentration. Figure 4.1 shows the synthetic grain packs that were constructed to examine the permeability behavior of such cases. Grain packs shown in the left column exhibit a greater fraction of large grains, while grain packs on the right column exhibit a

greater fraction of small grains. Permeability is then calculated for all of the samples, thereby enabling the estimation of the cementation exponent using equation (4.4).

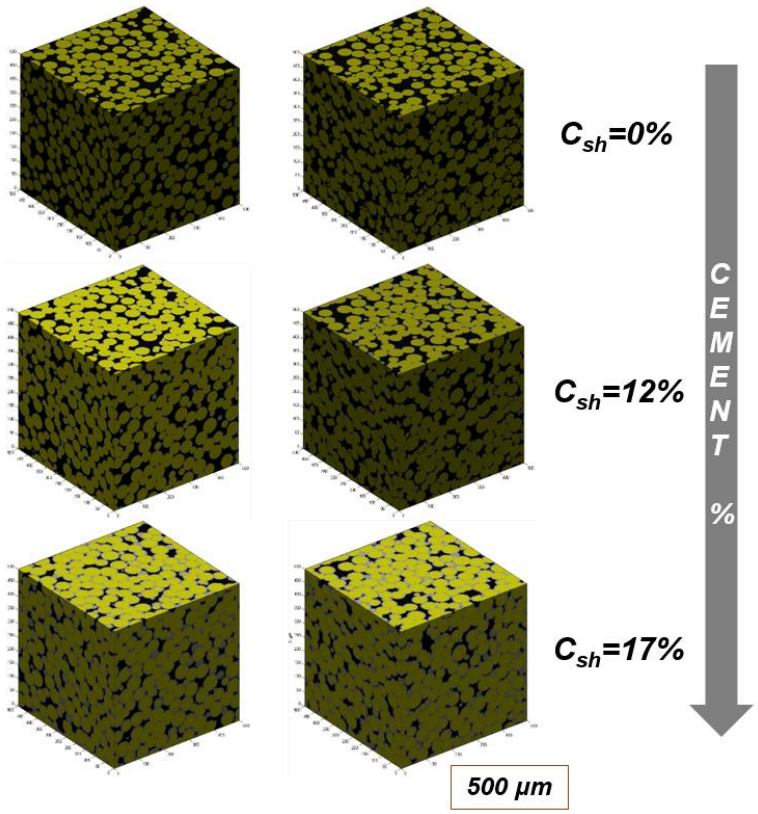

Figure 4.1: Synthetic grain packs constructed with UTAPWeLS's Pore Level Petrophysics module (Shabro, 2013, and Torskaya, 2014) to estimate the permeability in mixed grains and shale systems with dispersed topology. Different volumetric fractions of cement were added as an approximation for the dispersed shale concentration in order to calculate permeability for different shale concentrations.

4.2 THREE-DIMENSIONAL CHART RELATING PERMEABILITY, ROCK TYPE FRACTION, AND SHALE CONCENTRATION.

In the previous section, equations were derived to calculate the permeability of rocks that exhibit variable grain sizes. Two cases were introduced, where different grain

types were arranged in laminae and also where they were randomly distributed in the rock. Figure 4.2 contains a graphical representation of the equations derived in the previous section. The three-dimensional chart relates the rock type fraction, shale concentration, and permeability for both laminated and dispersed shale systems. From the chart an interesting relationship can be observed between the permeability and shale topology. For the case of dispersed topology, rocks containing small concentrations of shale show a rapid decrease in permeability. Conversely, in the laminated shale-sandstone system the decrease in the parallel to bedding plane permeability is not as steep. This chart demonstrates that an accurate assessment of grain topology is necessary for reliably calculating the flow properties of a given sample.

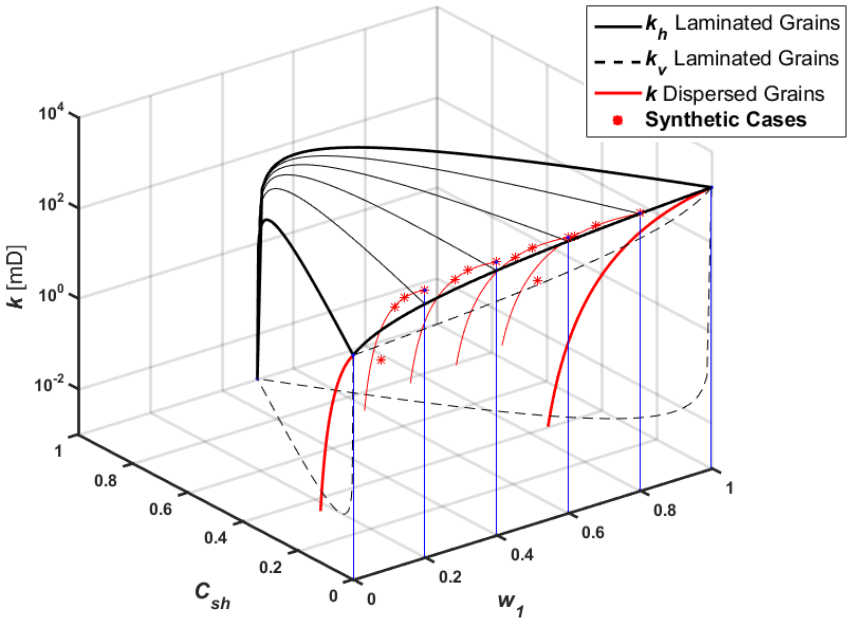

Figure 4.2: Three-dimensional chart relating volumetric fraction of grain type, shale concentration, and permeability. Two cases are considered when the components are arranged in a (i) laminated (black lines), and (ii) dispersed (red lines) fashion.

4.3 Impact of Grain Topology on Capillary Pressure

Bimodal grain-size distributions will not necessarily exhibit a bimodal throat-size distribution. There is a determining factor for the relationship between these two properties, which is grain topology. When there are two different rock types within a given sample, these grains can be spatially arranged in many different ways. In this section, I explore the behavior of two extreme cases: when the two rock types are arranged as two laminae, and when both are randomly arranged in a dispersed fashion.

The goal is to assess the type of throat-size distribution resulting from the two cases. To achieve this goal, I constructed synthetic rock cases using the UTAPWeLS Pore-Level Petrophysics module. Accordingly, I simulated the throat-size distribution corresponding with a given bimodal grain-size distribution. In the first case, the two grain-size modes were arranged in a laminated distribution, and in the second case they were arranged in a randomly dispersed distribution. Using a finite-difference geometrical pore approximation method (Shabro, 2013, and Torskaya, 2014), the simulator calculates the permeability and corresponding throat-size distributions in the X, Y, and Z-directions. Flow occurring in the X and Y directions corresponds with the parallel to bedding plane orientation while flow in the Z-direction represents the perpendicular to bedding plane orientation. Figure 4.3 displays the synthetic grain packs representing the (i) laminated and (ii) dispersed distributions.

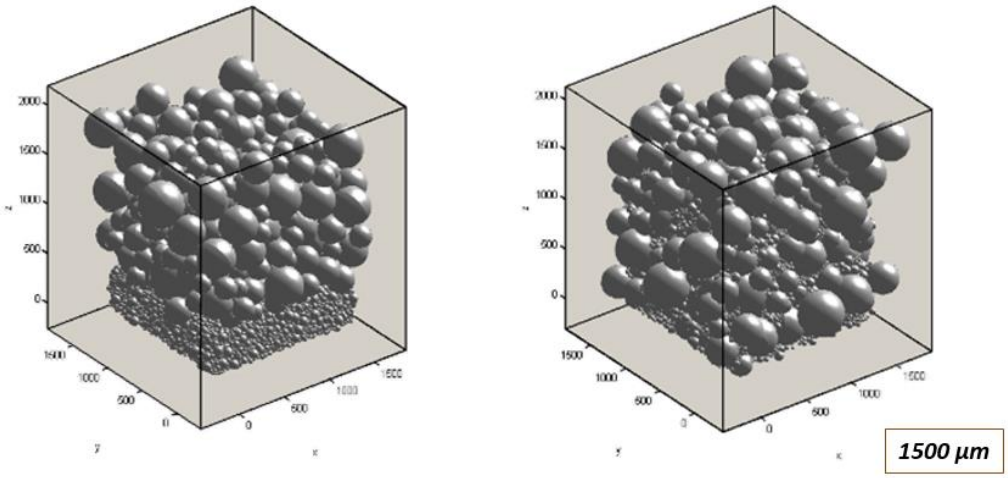

Figure 4.3: Synthetic grain packs with a constant grain-size distribution, but different grain topologies. The sample on the left has a laminated topology and the one on the right has an array of dispersed grains.

Figure 4.4 shows the calculated throat-size distributions for both the laminated (Fig. 4.4a) and dispersed (Fig. 4.4b) cases. Although a constant grain-size distribution was used for the two cases, it was observed that the throat-size distributions varied significantly. For the dispersed case the throat-size distribution exhibits a single dominant peak. However, the calculated throat-size distribution for the laminated case exhibits two distinct modes, which confirms that different grain sizes can indeed result in a bimodal throat-size distribution if they are arranged with a laminated grain topology.

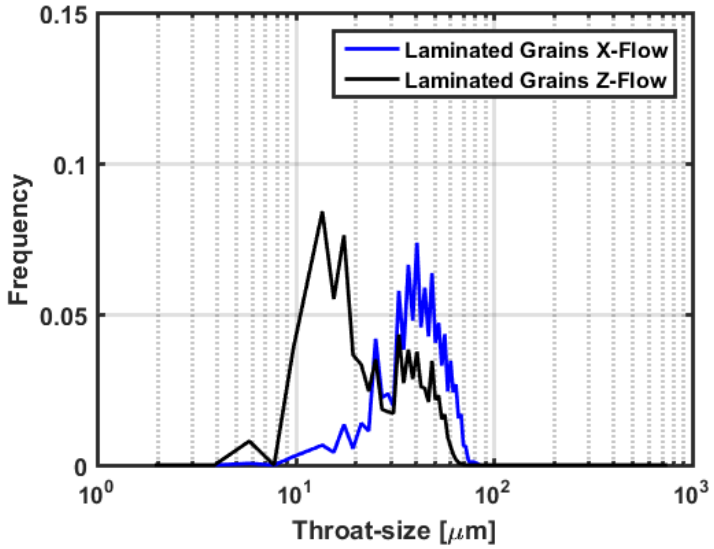

(a)

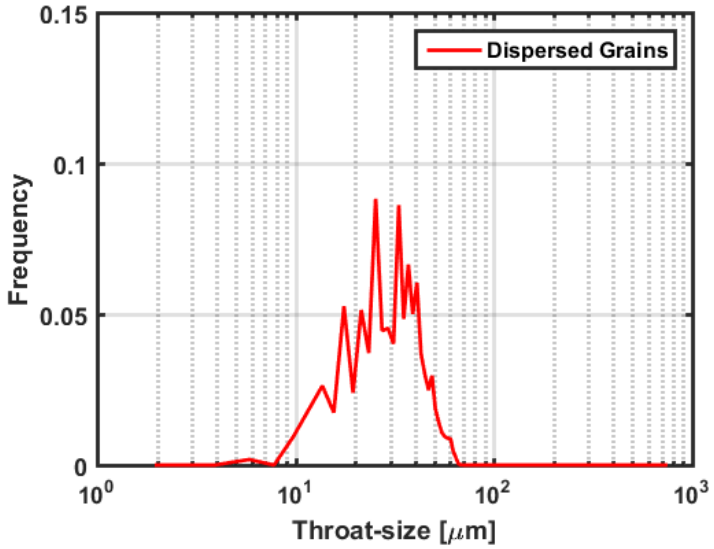

(b)

Figure 4.4: Calculated throat-size distributions of a rock sample that exhibits a bimodal grain-size distribution with grain sizes arranged in (a) laminated fashion and in (b) dispersed fashion. It follows that bimodal throat-size distributions can result from rocks exhibiting a laminated grain topology.

Chapter 5: Petrophysical Rock Classification[3]

I present two methods for improved petrophysical rock classification. In the first method, the parameters obtained from the basis functions are averaged to calculate a characteristic mean that is representative of the complete pore space. In the second method, each mode of the throat-size distribution is clustered independently to assess the different rock types based on their storage and flow properties. I show applications of these two methods in carbonate and tight-gas sandstone field cases. I compare my results with existing rock classification procedures to understand where the methods introduced in this thesis yield improved results.

5.1 Method 1: Weighted Average of Modeling Parameters

The first rock classification method considered here consists of obtaining a characteristic mean parameter that is representative of the complete bimodal throat space. This is achieved by calculating a weighted average of the pore-throat geometry parameters obtained from the MICP modeling process. Subsequently, the characteristic mean throat radius and amplitude parameters are calculated and used in the clustering analysis.

5.1.1 Obtaining a Characteristic Mean Throat Size or Mean Particle Diameter

As an example of how the characteristic mean throat size parameter is obtained, I calculate the mean throat size for a bimodal throat-size distribution. Equation (3.2) described this calculation for a throat-size distribution. When grain size data are available, one can calculate the characteristic mean particle diameter using

[3] Content from this Chapter was previously published by the main author (Palavecino et al., 2016).

$$D_m^2 = w_1 D_{o1}^2 + w_2 D_{o2}^2, \tag{5.1}$$

where D_m is the characteristic mean particle diameter of the system, D_{o1} and D_{o2} are the mean particle diameters of the large and small grain size modes, respectively, and w_1 and w_2 are the pore-volume fractions corresponding with each of the modes.

In a similar approach, a characteristic amplitude parameter that represents the complete pore-throat system is given by

$$\gamma_m^2 = \gamma_1^2 w_1 + \gamma_2^2 w_2, \tag{5.2}$$

where γ_m is the characteristic amplitude parameter for the case of the Lorentzian model and γ_1 and γ_2 are the amplitude parameters of the large and small grain size or throat size modes, respectively.

5.1.2 Clustering and Results: Field Cases 1 and 2

After estimating all the fitting parameters described in chapters 2 and 3, via least-squares regression, I complete the study by performing rock classification. The parameters obtained from each model are used to implement K-means clustering analysis (Press et al., 2007). An optimal number of rock classes is assessed with a silhouette plot (Rousseeuw, 1987). Subsequently, I introduce a rock classification method based on (a) mean throat radius, (b) throat-size distribution, and (c) total pore volume. This procedure can be repeated for any of the three parametric models introduced earlier in this thesis. Figure 5.1 shows the rock classification results for the carbonate Panoma field. Available samples were classified into a total of five rock classes. The FZI (Amaefule et al., 1993) method is included for comparison to results obtained from the various parametric models. Both the bimodal Lorentzian and Gaussian models yield better rock classification results than Thomeer's or FZI models. The FZI method yields a steep permeability/porosity

relationship that erroneously clusters together rock samples which have very different textural properties. Because the Lorentzian and Gaussian methods include the dominant throat radius along with the throat-size distribution amplitude and the total pore volume, they yield rock classification results that are more petrophysically consistent.

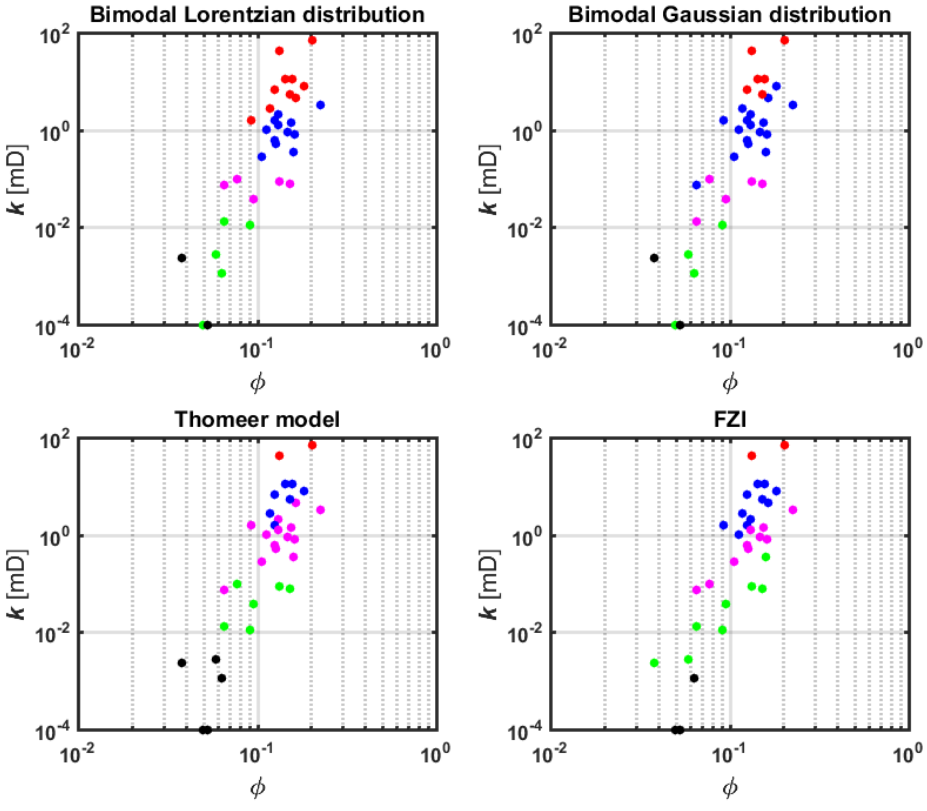

Figure 5.1: Rock classification results for Field Case 1: Panoma carbonates. Rock classification results were obtained using the three bimodal parametric models described in this thesis (Chapter 2). Colors represent different clusters, which rank from the highest quality rock type (red) to the lowest quality rock type (black). A comparison to Amaefule's FZI classification is shown. FZI classification shows a relatively steep permeability/porosity relationship that erroneously clusters together rock samples that have very different textural properties.

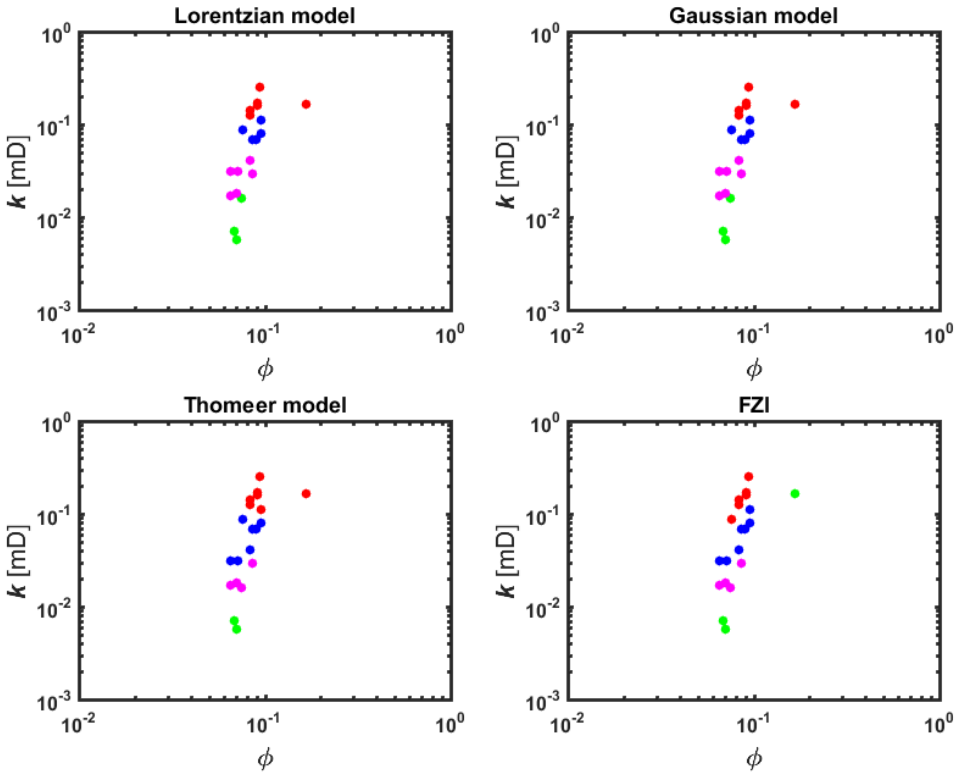

Figure 5.2: Rock classification results for Field Case 2: Bossier tight-gas sandstone. Rock classification results were obtained using the three bimodal parametric models described in this thesis (Chapter 2). Colors represent different clusters, which rank from the highest quality rock type (red), to the lowest quality rock type (green). A comparison to Amaefule's FZI classification is shown. FZI classification shows a data point with high porosity and permeability clustered in the lowest quality category (green), while it is clustered in the best class by the models introduced in this thesis.

5.2 Method 2: Individualized Throat-Size Distribution Modes

The second rock classification method includes the concept of grain topology in the rock typing procedure. In chapter 4, I examined how grain topology affect capillary pressure. Based on those findings, when a clastic rock exhibits a bimodal throat-size distribution, two different flow systems exist that can be treated independently. The second

rock classification method focuses on the individualization of the two flow systems and takes that into account to implement a rock typing workflow.

5.2.1 Laminations of different grain sizes: Individualizing the flow systems

MICP data was modeled using Lorentzian probability density functions (Palavecino et al., 2016). This method allows one to individualize the different modes present in the bimodal throat-size distribution of each sample. Figure 5.3 shows how MICP modeling is done, and how each mode of the throat-size distribution is individualized. As discussed in chapter 4, I assume that the above bimodality occurs because two distinct sandstone types are present within the sample, especially when they are arranged in a laminated fashion.

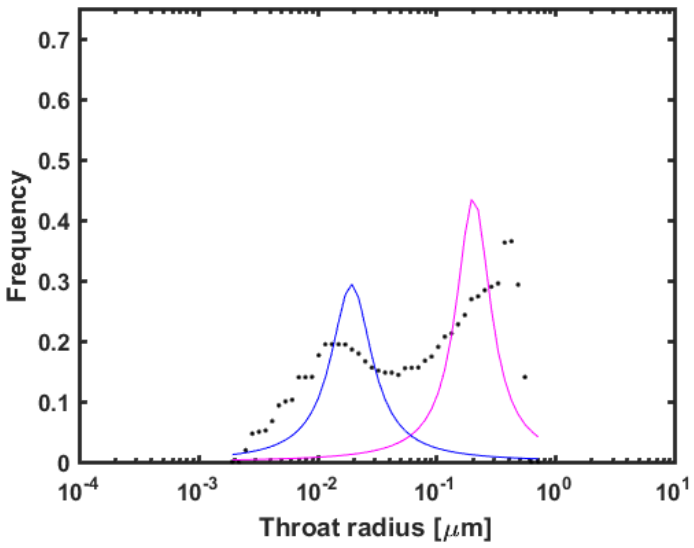

Figure 5.3: Example of how each field case sample is modeled using a bimodal Lorentzian probability density function. The modes of the throat-size distribution are separated and clustering is performed with all of the individual modes for further rock classification.

5.2.2 Clustering via Decoupled Throat-Size Modes: Field Case 4

I perform K-means clustering analysis (Press et al., 2007) for all of the independent parameters of each mode. Each of the individual modes will be assigned to a cluster, representing a given rock type, as shown in Fig. 5.4. Different samples were then classified into four final clusters by recombining the modes.

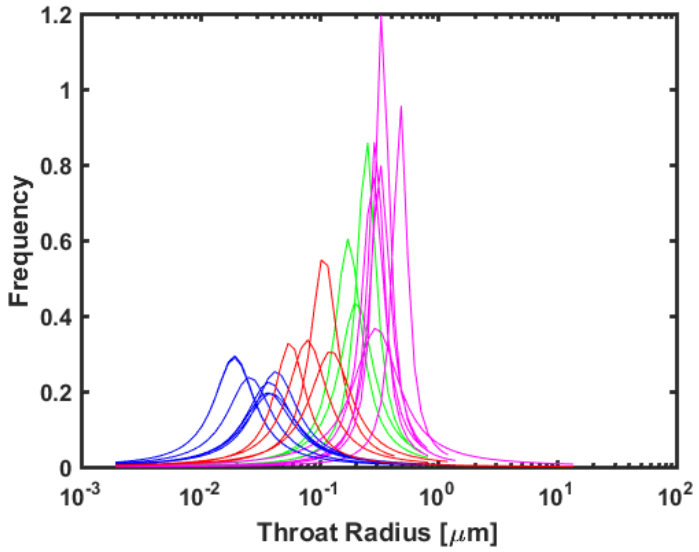

Figure 5.4: Individualized throat-size distributions from the tight-gas sandstone field case. Colors represent the four rock types, ranking from the highest quality rock type (magenta) to the lowest quality rock type (blue).

Finally, Fig. 5.5 describes the classified samples, via a permeability-porosity-irreducible water saturation plot. Figure 5.6 compares these results with Winland's R35 classification (Pittman, 1992). The rock classification method introduced above yields well defined clusters that can be used to improve the estimation of permeability or irreducible water saturation. However, Winland's method does not provide good results for this

example because it fails to account for the bimodal nature of the throat-size distributions. This erroneous assumption results in the different rock classes being mixed with no clear trend in the permeability-porosity-irreducible water saturation plot.

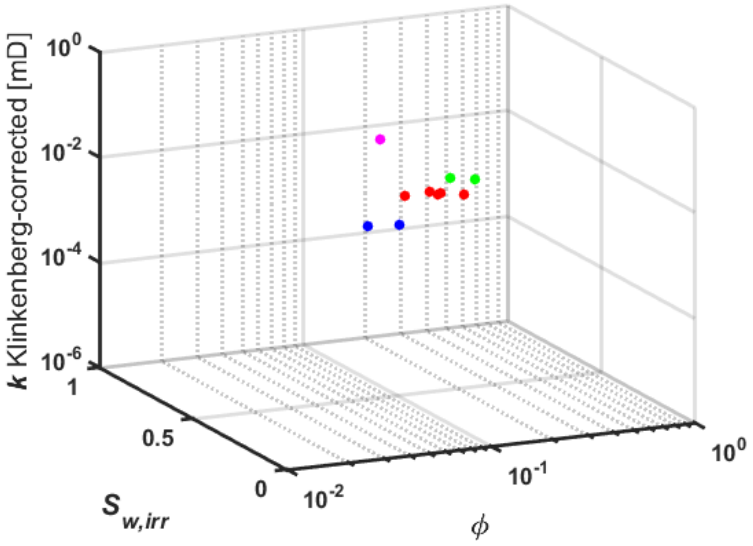

Figure 5.5: Rock classification results obtained using the second method presented in this thesis. The results are shown in a 3D porosity, irreducible water saturation, permeability chart. Each color represents a given cluster ranking from the highest quality rock type (magenta) to the lowest quality rock type (blue).

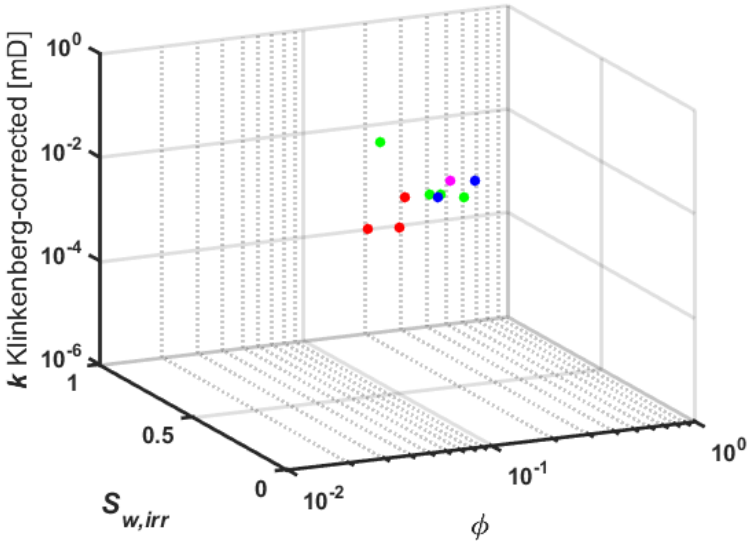

Figrue 5.6: Winland's R35 classification results obtained for the same field case shown in Fig. 5.5. The clustering analysis using Winland's method does not yield well-defined rock classes. It follows that Winland's method fails to produce accurate rock classification results because it does not reproduce the bimodal throat-size distribution present in the sample.

Chapter 6: Conclusions

I invoked three parametric models to reproduce MICP and grain-size distribution measurements. The parametric models were specifically designed to accommodate bimodal distributions. Reliable correlations with permeability and irreducible water saturation were derived using the fitting parameters associated with each of the models. Application to several field examples indicates that the basis functions introduced in this work improve rock classification results for cases where rocks exhibit a bimodal grain/pore-size distribution. It was also verified that the new models result in better estimates of petrophysical properties compared to conventional methods. Calculations showed that bimodal throat-size distributions in clastic rocks result from the presence of variable grain sizes arranged in a laminated fashion. Making use of synthetic pore-scale simulations, I demonstrated that different grain sizes arranged in a dispersed fashion would yield a unimodal throat-size distribution, yet with a wider amplitude.

For the case of unimodal rocks with narrow throat and grain-size distributions, conventional methods will invariably yield similar classification results as the methods introduced in this thesis. The new parametric models can take into account arbitrary non-symmetric and bimodal pore/throat-size distributions that arise in spatially complex rocks, such as carbonates and tight-gas sandstones, for the calculation of permeability. However, in clastic rock systems, it is important to assess whether the bimodality of throat sizes does or does not originate from grain size laminations, prior to implementing the basis functions described in this work.

The models introduced in this thesis can be easily applied to any rock characterization workflow. An accurate rock classification procedure enables a better estimation of permeability, resulting in improved calculations of the rock's productivity.

Finally, a better description of the different rock types present in the formation improves the construction of a reservoir model and allows for a more accurate estimation of hydrocarbon reserves.

Core-based rock classification methods based on high quality data produce very accurate results and they represent a fundamental step in the study of rock typing. However, core data is often not readily available due to the high acquisition and processing costs associated with it. Future research efforts should be made in order to translate the core-based classification methods presented in this thesis to log-based classification methods that would expand the accuracy of these methods to a larger scale.

Glossary

A_{bt} : Fitting parameter to experimental data in the bundle of capillary tubes model, [mD]

A_{kc} : Fitting parameter to experimental data in the Kozeny-Carman model, [mD]

B_{bt} : Fitting parameter to experimental data in the bundle of capillary tubes model, [mD/($microns^2$)]

B_{kc} : Fitting parameter to experimental data in the Kozeny-Carman model, [mD/ $(microns)^2$]

BV : Bulk Volume, [%]

$BV_{\infty 1}$: Bulk volume infinite of hyperbola 1, [%]

$BV_{\infty 2}$: Bulk volume infinite of hyperbola 2, [%]

C_{bt} : Fitting parameter to experimental data in the irreducible water saturation estimation from MICP, [$microns^2$]

C_{kc} : Fitting parameter to experimental data in the irreducible water saturation estimation from grain size data, [microns]

C_{sh} : Shale concentration, [fr.]

D_{o1} : Mean particle diameter of mode 1, [microns]

D_{o2} : Mean particle diameter of mode 2, [microns]

D_p : Particle diameter, [microns]

D_{pm} : Average grain diameter, [microns]

FZI : Flow zone indicator

G_1 : Thomeer's geometric parameter of hyperbola 1, [dimensionless]

G_2 : Thomeer's geometric parameter of hyperbola 2, [dimensionless]

$Hg - P_c$: Mercury capillary pressure, [psi]

k : Permeability, [mD]

k_h : Effective parallel to bedding plane permeability, [mD]

k_{sd} : Permeability of the sandstone, [mD]

k_{s1} : Permeability of the sandstone type 1, [mD]

k_{s2} : Permeability of the sandstone type 2, [mD]

k_{sd12} : Effective permeability of the mixed-sandstone fraction, [mD]

k_{sd-sh} : Effective permeability of the shaly-sandstone system, [mD]

$k_{sd12-sh}$: Effective permeability of the mixed-sandstone-shale system, [mD]

k_{sh} : Permeability of the shale, [mD]

k_v : Effective perpendicular to bedding plane permeability, [mD]

m_{cs} : Cementation exponent of the rock, [dimensionless]

m_{cs12} : Cementation exponent of the mixed-sandstone-shale system, [dimensionless]

$MICP$: Mercury-Intrusion Capillary Pressure

NMR : Nuclear Magnetic Resonance

P_c : Capillary pressure, [psi]

P_{d1} : Displacement pressure of hyperbola 1, [psi]

P_{d2} : Displacement pressure of hyperbola 2, [psi]

R : Throat radius, [microns]

R_m : Characteristic mean throat radius, [microns]

R_{o1} : Mean throat radius of mode 1 of the Lorentzian distribution, [microns]

R_{o2} : Mean throat radius of mode 2 of the Lorentzian distribution, [microns]

S_{Hg} : Mercury saturation, [fr.]

S_w : Wetting phase saturation, [fr.]

$S_{w,irr}$: Irreducible water saturation of the rock, [fr.]

UTAPWeLS: The University of Texas at Austin Petrophysical and Well-Log Simulator

w_1 : Pore volume fraction of mode 1, [fr.]

w_2 : Pore volume fraction of mode 2, [fr.]

γ_1 : Scale (amplitude) parameter of mode 1, [dimensionless]

γ_2 : Scale (amplitude) parameter of mode 2, [dimensionless]

γ_m : Characteristic amplitude parameter of the Lorentzian model, [dimensionless]

θ : Contact angle, [radians]

μ_1 : Mean throat radius of mode 1 of the Gaussian distribution, [microns]

μ_2 : Mean throat radius of mode 2 of the Gaussian distribution, [microns]

σ : Surface tension, [N/m]

σ_1 : Standard deviation of mode 1 of the Gaussian distribution, [dimensionless]

σ_2 : Standard deviation of mode 2 of the Gaussian distribution, [dimensionless]

τ : Tortuosity of the rock, [dimensionless]

ϕ : Porosity of the rock, [fr.]

ϕ_{sd} : Porosity of the sandstone, [fr.]

ϕ_{sd12} : Porosity of the mixed sandstone system, [fr.]

ϕ_{sh} : Porosity of the shale, [fr.]

References

Amaefule, J. O., Altunbay, M., Tiab, D., Kersey, D. G., and Keelan, D. K., 1993, "Enhanced Reservoir Description: Using Core and Log Data to Identify Hydraulic (Flow) Units and Predict Permeability in Uncored Intervals/Wells", SPE 68th Annual Technical Conference and Exhibition, Houston, October.

Dubois, M. K., Byrnes, A. P., Bhattacharya, S., Bohling, G. C., Doveton, J. H., and Barba, R. E., 2006, "Hugoton Asset Management Project (HAMP): Hugoton Geomodel Final Report", KGS Open File Report.

Johnson, N. L., Kotz, S., and Balakrishnan, N., 1994, Continuous Univariate Distributions, Wiley, New York.

Montgomery, S., 2000, East Texas Basin Bossier gas play, Petroleum Frontiers 17, 2, IHS Energy Group, Englewood.

Palavecino, M. and Torres-Verdín, C., 2016, "New method of petrophysical rock classification based on MICP and grain-size distribution measurements", SPWLA 57th Annual Symposium, Reykjavik, Iceland, June.

Peters, E. J., 2012, Advanced Petrophysics, Greenleaf Book Group, Austin.

Pittman, E. D., 1992, "Relationship of Porosity and Permeability to Various Parameters Derived from Mercury Injection-Capillary Pressure Curves for Sandstone", AAPG Bulletin 76, 2, pp. 191-198.

Press, W. H., Teukolsky, S. A., Vetterling, W. T., and Flannery, B. P., 2007, Numerical Recipes: The Art of Scientific Computing, Gaussian mixture models and k-means clustering, Cambridge University Press, New York.

Revil, A. and Cathles, L. M., 1999, "Permeability of shaly sands". Water Resources Research 35, 3, pp. 651-662.

Rousseeuw, P. J., 1987, "Silhouettes: a graphical aid to the interpretation and validation of cluster analysis", Journal of computational and applied mathematics 20, pp. 53-65.

Shabro, V., 2013, "Pore-scale numerical modeling of petrophysical properties with applications to hydrocarbon-bearing organic shale", Doctoral Dissertation, The University of Texas at Austin, URI: http://hdl.handle.net/2152/22902.

Thomeer, J. H. M., 1960, "Introduction of a Pore Geometrical Factor Defined by the Capillary Pressure Curve", AIME 219, pp. 354-58.

Timur, A., 1968, "An Investigation of Permeability, Porosity, and Residual Water Saturation Relationships", SPWLA 9th Annual Logging Symposium, New Orleans, June.

Torskaya, T.S., 2014, “Pore-scale analysis of grain shape and sorting effect on fluid transport phenomena in porous media”, Doctoral Dissertation, The University of Texas at Austin, URI: http://hdl.handle.net/2152/23093.

Xu, C. and Torres-Verdín, C., 2013, “Pore System Characterization and Petrophysical Rock Classification Using a Bimodal Gaussian Density Function”, Mathematical Geosciences 45, 6, pp. 753-771.

Vita

Mauro Palavecino is currently a M.Sc. Petroleum Engineering candidate at The University of Texas at Austin. His research work focuses on studying different rock classification methods that improve the petrophysical description of rocks with complex pore-geometries, such as carbonates and tight-gas sandstones. He received his B.Sc. in Chemical Engineering from the National University of La Plata, Argentina in 2012. Prior to joining the Formation Evaluation Research Consortium group at The University of Texas at Austin, he worked for Sinopec Argentina Exploration and Production as Reservoir Engineer from 2011-2014. Mauro is an active member of the Society of Petrophysicists and Well Log Analysts (SPWLA), where he serves as Public Relations Director for the Student Chapter at The University of Texas at Austin.

Permanent email: mpalavecino@utexas.edu

This thesis was typed by Mauro Ariel Palavecino.